Search for Gravitational Wave radiation associated with the pulsating tail of the SGR 1806-20 hyperflare of December 27 2004 using the LIGO observatory

LIGO collaboration

We have searched for Gravitational Waves (GWs) associated with the SGR 1806-20 hyperflare of December 27 2004, a close-by source which displayed exceptional energetics. Recent investigations on the lightcurve pulsating tail revealed the presence of Quasi-Periodic Oscillations (QPOs) in the $30-2000$Hz frequency range, most of which coincided with the bandwidth of the LIGO observatory. These QPOs, with well-characterized frequencies, are plausibly being attributed to seismic modes of the neutron star. Our search targeted potential quasi-monochromatic GWs lasting for tens of seconds and emitted at the QPO frequencies and their second harmonics. We have observed no candidate events above a pre-determined threshold and our best upper limit corresponds to $h_{rss}^{90\%} = 5.63 \times 10^{-22}$strain$/\sqrt{\text{Hz}}$ on the GW waveform strength in the detectable polarization state reaching our Hanford (WA) detector. We illustrate the astrophysical significance of the result via the characteristic energy of the allowed GWs at the source using a simple source model. Our best result corresponds to $6.63 \times 10^{-8} M_{sun} c^2$, which is a factor of a few away from the total (isotropic) energy emitted in the electromagnetic spectrum. This is the best upper limit published to our knowledge and represents the first multiple-frequency astero-seismology measurement using a GW detector.

PACS numbers:

I. INTRODUCTION

Soft γ-ray Repeaters (SGRs) are thought to be neutron stars that emit short-duration X and γ-ray bursts at irregular intervals (see [1] for a review). These recurrent bursts generally have durations of the order of ~ 100ms and luminosities in the $10^{39} - 10^{42}$erg/s range. At times, though rarely, these sources emit giant flares lasting hundreds of seconds (see for example [2–4]) with peak luminosities reaching 10^{47}erg/s [5]. Pulsations in the lightcurve tail reveal the neutron star spin period.

Several characteristics of SGRs can be explained in terms of the *magnetar* model[9], highly magnetised isolated neutron stars ($B \sim 10^{15}$G). In the context of this model the giant flares are generated by the catastrophic rearrangement of the neutron star crust and magnetic field plausibly exciting seismic modes of the star[10].

Quasi-Periodic Oscillations (QPOs) in the pulsating tail of giant flares were first observed for the December 27 2004 event of SGR 1806-20 by the *Rossi X-Ray Timing Explorer (RXTE)* and *Ramaty High Energy Solar Spectroscopic Imager (RHESSI)* satellites [6–8]. Prompted by the above observations, the RXTE data from the SGR 1900+14 giant flare of August 27 1998 was revisited[11] and transient QPOs were found in the lightcurve pulsating tail at similar frequencies (also rotation phase dependent) to the SGR1806-20 event, suggesting that the same fundamental physical process is likely taking place.

It has been suggested that the star's seismic modes might drive the observed QPOs[6–8], which leads us to investigate a possible emission of GWs associated with them. There are several classes of non-radial neutron star seismic modes with characteristic frequencies in the $\sim 10 - 2000$Hz range[12]. Toroidal modes of the neutron star crust are expected to be excited by large crustal fracturing (see [6–8, 13]), though these modes may be poor GW emitters. However, crust modes could magnetically couple to the core's modes possibly generating a GW signal accessible with today's technology (see [14–16]). Alternative modes with expected frequencies in the observed range are crustal interface modes, crustal spheroidal modes, crust/core interface modes or perhaps p-modes or f-modes. The latter should, in theory, be stronger GW emitters ***(REF HERE)***. The exceptional energetics of the hyperflare[4, 17], the close proximity of the source[4, 18–20] and the availability of precisely measured QPO frequencies and bandwidths [6–8] also made this source very attractive.

In this paper we make use of the LIGO Hanford (WA) 4km detector (H1) to search for or to place an upper bound on the Gravitational Wave (GW) emission associated with the observed QPO phenomena.

II. SATELLITE OBSERVATIONS

SGR 1806-20 is a galactic X-ray star thought to be at a distance of $d = 10 - 15$kpc[4, 18–20]. The total (isotropic) flare energy for the December 27 2004 record flare was measured to be $\sim 10^{46}$ergs[4, 17].

QPOs in the pulsating tail of the SGR 1806-20 hyperflare were first observed by Israel *et al.*[8] using RXTE. These observations revealed oscillations centered at ~ 18, ~ 30 and ~ 92.5Hz, associated with a particular rotation phase of the star. Using RHESSI, Watts and Strohmayer[6] confirmed the QPO observations of Israel *et al.* revealing an additional frequency at 626.5Hz associated with a different rotational phase. Closer inspection of the RXTE data by Strohmayer and Watts[7] revealed a richer presence of QPOs, identifying a significant component at 150 and 1840Hz as well. Tab.(I) is taken from ref.[7] and summarizes the properties of the most signif-

Observation	Frequency [Hz]	FWHM [Hz]	Period [s]	Satellite	References
a	17.9 ± 0.1	1.9 ± 0.2	60-230	RHESSI	[6]
b	25.7 ± 0.1	3.0 ± 0.2	60-230	RHESSI	[6]
c	29.0 ± 0.4	4.1 ± 0.5	190-260	RXTE	[7]
d	92.5 ± 0.2	$1.7^{+0.7}_{-0.4}$	170-220	RXTE	[8]
e	”	”	150-260	”	[7][a]
f	92.7 ± 0.1	2.3 ± 0.2	150-260	RHESSI	[6]
g	92.9 ± 0.2	2.4 ± 0.3	190-260	RXTE	[7]
h	150.3 ± 1.6	17 ± 5	10-350	RXTE	[7]
i	626.46 ± 0.02	0.8 ± 0.1	50-200	RHESSI	[6]
l	625.5 ± 0.2	1.8 ± 0.4	190-260	RXTE	[7]
m	1837 ± 0.8	4.7 ± 1.2	230-245	RXTE	[7]

[a] ref.[7] makes an adjustment to the observation times of ref.[8]

TABLE I: Summary of the most significant QPOs observed in the pulsating tail of SGR 1806-20 during the December 27 2004 hyperflare (from ref.[7]). The duration of the QPO transient is measured with respect to the flare peak, the frequencies are given from the Lorenzian fits of the data and the width corresponds to the Full-Width-at-Half-Maximum (FWHM) of the QPO structure.

icant QPOs detected in the lighcurve tail of the SGR 1806-20 giant flare.

III. THE LIGO DETECTORS

Outline to be completed

- *Brief description of the detector, state close to S4, however under commissioning. At the time of the event, only one of the three LIGO detectors (the* 4km *long interferometer H1, located at Hanford (WA)) was collecting data and for this reason the search is adapted to use only one data stream.* **(REF HERE)**
- *Brief description of the Astrowatch program* **(REF HERE)**
- *Precise definition of the lock stretch containing the flare is analyzed (due to commissioning)*
- *Description of H1 calibration* **(REF HERE)**
- *Sensitivity curve, frequency band of sensitivity at the time of the event.* **(REF HERE)**

IV. DATA ANALYSIS

This analysis relies on a variant of the sensitive *excess power*[21–23] algorithm comparing time-frequency slices at the time of the observations against neighboring ones. The algorithm is adapted to analyze a single data stream at multiple frequency bands and it is expandable to handle multiple coincident data streams as well. The trigger provided for the analysis corresponds to the flare's X-ray peak as provided by the GRB Coordinate Network (GCN) reports n.2920[27] and 2936[28] corresponding to 788218239 GPS seconds.

In the absence of reliable theoretical models, we keep the GW search as broad and sensitive as possible. The search follows the QPO signatures observed in the electromagnetic spectrum both in frequency and time duration. In particular, we measure the power for the observed durations at the observed QPO frequencies (as shown in tab.(I)) for a given bandwidth (mostly 10 Hz) and we compare it to the power measured in adjacent frequency bands not related to the event. The *excess power* is then calculated for each time-frequency volume of interest.

According to the present consensus, the hyperflare is attributed to a *starquake*[17, 24] on the neutron star crust and the mode excitation is expected to begin at the time

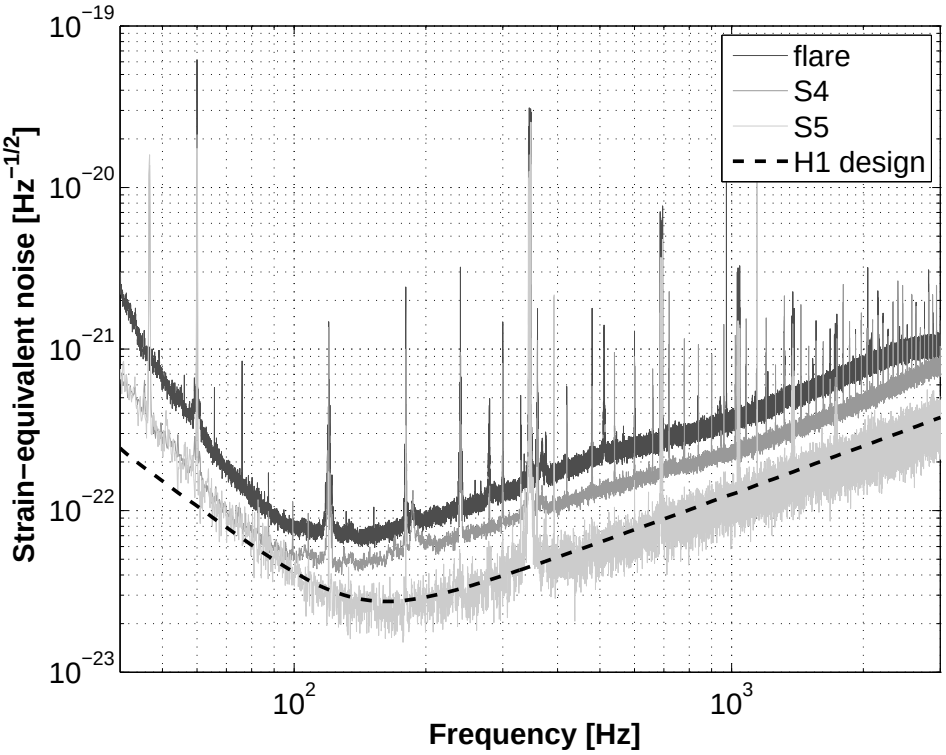

FIG. 1: ciao

of the flare. Therefore, besides search durations determined by the satellite observation times (tab.(I)), we also search for GW emission associated with the proposed seismic modes from the received trigger time of the event. In addition to the above measurements, we also address a plausible emission at twice the QPO frequency.

Another aspect of the satellite observations is the quasi-periodic nature of the emitted electromagnetic waveform with possible slow drift in frequency. Although there is no knowledge of GW waveforms associated with this type of event, we tune our search algorithm to be most sensitive to long quasi-periodic waveforms with fairly narrow bandwidth while short bursts are strongly discriminated against. The waveform set chosen to test the sensitivity of the algorithm via injections is chosen in line with this argument.

A. Pipeline

A block diagram of the the analysis pipeline is shown in fig.(2) where the GCN reports provide the trigger for the analysis. The *on* and *off*-source data regions are then selected where the former corresponds to the QPO observation periods, as shown in tab.(I). The *off*-source data region begins at the end of the six minute long QPO tail (set to 400s after the flare peak) lasting to ten minutes prior to the end of the stable H1 lock stretch for a total of $\sim$ 2h of background data.

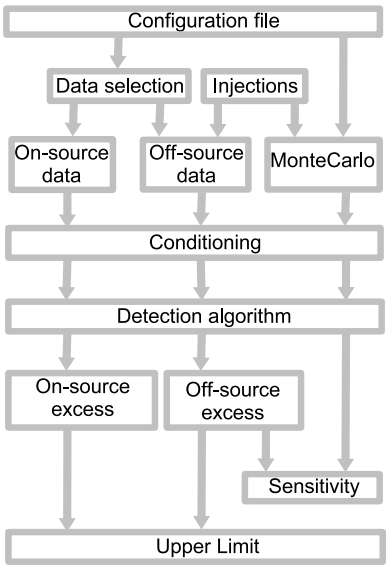

FIG. 2: A block diagram of the analysis.

The on-source region always consists of a single segment starting at the beginning of the QPO observation $t_{\rm qpo}$ and lasting for a period $\delta t_{\rm qpo}$ determined by the duration of the observation. The off-source region consists of numerous non-overlapping segments each of duration $\delta t_{\rm qpo}$.

To provide an estimate of the search sensitivity, an

arbitrary waveform can be injected and added to each off-source segment. All of the segments (*on-* or *off*-source) are processed identically. In the procedure described by the conditioning block, the data is band-pass filtered to select the three frequency bands of interest: the QPO band as shown on tab.(I) and the two adjacent frequency bands. Using the interferometer response function at the time of the event, the data is calibrated into units of strain and a data quality procedure is applied to the data set.

After the conditioning procedure is complete, the data stream is put through the detection algorithm, which computes the power in each segment for the three frequency bands of interest and then the excess power in the segment. The Feldman-Cousins[25] statistical approach is then used to place an upper limit based on the loudest event.

In order to check the complete signal flow the off-source segments can also be replaced with white Gaussian and stationary noise.

B. Data conditioning

The conditioning procedure consists of filtering the data with three different band-pass Infinite Impulse Response (IIR) Butterworth filters. The first band-pass filters the data around the QPO frequency of interest with a predefined bandwidth. This bandwidth depends on the observed QPO width (see tab.(I)) and on the fact that the QPOs have been observed to evolve in frequency. For the QPOs addressed here, the bandwidth is set to 10Hz with the exception of the 150.3Hz oscillation where the bandwidth is set to 17Hz.

The data is also filtered to select the two adjacent frequency bands with identical bandwidths of the chosen QPO band. Using the adjacent frequency bands allows us to essentially discriminate against common non-stationary broad band noise, thereby increasing the search sensitivity as will be described in sec.(IV C).

The three data streams are calibrated in units of strain using a transfer function which describes the interferometer response to a differential arm length change.

The conditioning procedure ends with the identification of periods of significant sensitivity degradation. These periods are selected by monitoring the power in each of the three frequency bands in tiles less than a second long. If the power is above a set threshold in any of the three bands the tile in question is tagged. We veto and reject the tile in question: an abrupt power change in the second long time frame does not correspond to a GW candidate lasting tens to hundreds of seconds long.

To optimize this threshold we used 125ms and 1s long tiles and we injected different waveform families to determine the corresponding search sensitivity.

C. The search algorithm

The algorithm at the root of the search is a variant of the *excess power*[21–23] algorithm. It consists of taking the difference in power between a band centered at a frequency f and the average of the two frequency bands adjacent to the QPO frequency band, also of bandwidth Δf, typically centered at $f_\pm = f \pm \Delta f$.

Power measurements are performed in segments of duration Δt starting at time t where Δt corresponds to the GW signal period we are searching for (tab.(I)). The excess power $\Delta\mathcal{P}$ is then

$$\Delta\mathcal{P} = \mathcal{P} - \mathcal{P}_{\rm avg} \tag{1}$$

where $\mathcal{P}$ is the power in the QPO frequency band and $\mathcal{P}_{\rm avg} = (\mathcal{P}_+ + \mathcal{P}_-)/2$ is the power average between the lower and upper adjacent frequency bands. We refer to the set of $\Delta\mathcal{P}$ calculated over the off-source region as the *background*. The on-source region provides a single excess power measurement. The algorithm used offers the advantage, by virtue of eq.(1), of measuring power changes in the QPO band while rejecting a common power increase in all three bands.

This rejection process, namely the process described by eq.(1), is applied to power measurements in non-overlapping segments of short duration (< 1s), set in this work to $\Delta\tilde{t} = 250$ms. This choice is driven by the aim to discriminate not only against broadband *burst*-like events but also occasional non-stationary noise floor changes. The resulting set of $\Delta\mathcal{P}$ measurements are then averaged to calculate the excess power corresponding to the GW signal period of interest.

Different sets of more or less astrophysically-motivated waveforms, or in some cases completely *ad-hoc* waveforms, are injected in the background region and the resulting excess power is computed. The sensitivity of the search to a particular waveform is defined as the energy necessary to cause 90% of the resulting $\Delta\mathcal{P}$ to be above the background median. This choice of definition provides a *characteristic* waveform strength which, on average, should not be far from a 90% upper bound.

Assuming white gaussian stationary noise for the detector output, we approximate the sensitivity with the expression

$$h_{\rm rss}^{90\%} \simeq 1.25\ \tilde{h}(f)\ \left(\Delta f\ \Delta t\right)^{1/4} \tag{2}$$

where $\tilde{h}(f)$ is the strain-equivalent amplitude spectral density of the detector noise at frequency f, in units of strain/rHz, and Δf and Δt are the bandwidth and duration of the segment in question, in units of s and Hz.

V. SENSITIVITY OF THE SEARCH

We injected various waveform families, namely Sine-Gaussian (SG), White Noise Bursts (WNB), Amplitude

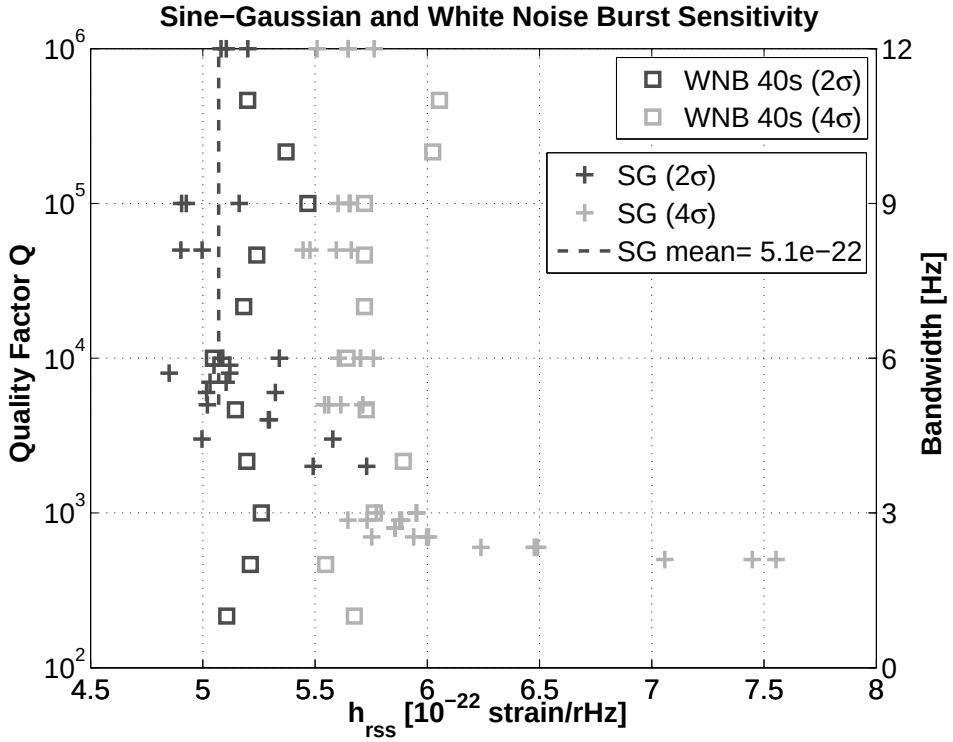

FIG. 3: Search sensitivity to SG waveforms (crosses) and WNB bursts (squares) as a function of different waveform parameters and data quality cuts. The cuts are relative to the background RMS distribution calculated in segments 125ms long. For the case of SG injections, the waveform quality factor is varied from $Q = 600$ to $Q = 10^6$ and the dashed line represents the average sensitivity ($5.1 \times 10^{-22}\text{strain}/\sqrt{Hz}$) for injections with $Q > 5 \times 10^3$ (where the response is essentially flat) and a 2σ cut. For the WNB case, 40s long bursts are injected with a bandwidth ranging from 1Hz to 11Hz. For the above parameter space the response is essentially constant.

(AM) and Phase Modulated (PM) waveforms, in the off-source region to quantify the sensitivity of the search to these types of waveforms. The strength of the injection h(t) is determined by calculating the *root-sum-square* (rss) defined as

$$h_{\rm rss} = \sqrt{\int_{-\infty}^{+\infty} |\mathrm{h(t)}|^2 \mathrm{dt}} \qquad (3)$$

Each waveform was added directly to the raw data segments and the search sensitivity was explored as a function of the various parameters. As previously mentioned, we designed the algorithm so as to be sensitive to waveforms with a preset small frequency range while discriminating against any types of short duration signals.

The result of the sensitivity study relative to the 92.5Hz QPO (observation *d* of tab.(I)) is shown in fig.(3) and fig.(4) where the band center frequencies, bandwidths and signal durations were set to $f = 92.5$Hz, $f_- = 82.5$Hz, $f_+ = 102.5$Hz, $\Delta f = 10$Hz and $\Delta t = 50$s.

The SG waveform is parameterized as follows

$$h = A\ \sin(2\pi f t + \phi)\ e^{(t-t_0)^2/\tau^2} \qquad (4)$$

where A is the waveform amplitude, f is the waveform frequency, $Q = \sqrt{2}\pi\tau f$ is the quality factor, ϕ is an arbitrary phase and t_0 indicates the waveform maximum. In the case of $Q \to \infty$ the waveform approaches the form of a pure sinusoid. Fig.(3) plots the search sensitivity versus the quality factor Q of the SG injection indicating that the analysis is most sensitive to SG waveforms with quality factors in the range $Q \in [\sim 10^3 : \infty]$. The response is also shown as a function of a 2σ and 4σ data quality cut on the background RMS distribution calculated in tiles 125ms long. The more aggressive 2σ cut yields significantly better results and was chosen for the 92.5Hz QPO analysis.

The decline in sensitivity as the Q decreases originates from the data quality procedure. As this parameter takes smaller values, the waveform energy begins to concentrate in shorter time scales and the conditioning procedure identifies and removes intervals of the injection which are above threshold. In the 2σ case, the sensitivity is relatively flat for $Q > 5 \times 10^3$ and the average response is $h_{\rm rss} = 5.1 \times 10^{-22}\text{strain}/\sqrt{Hz}$ also shown in the plot by the dashed line.

Also shown in fig.(3) is the sensitivity to WNBs, for a 2σ and 4σ cut, for 40s long burst durations and bandwidths ranging from 1Hz to 11Hz. The waveform is generated by band-passing white noise through a 2^{nd} order Butterworth filter with bandwidth defined at the -3dB

cutoff point and burst duration set by a Tukey window. As shown in the previous cases, the most aggressive 2σ cut outperforms the 4σ and no significant departure in sensitivity is seen for bandwidths up to 10-11Hz.

Fig.(4) plots the sensitivity to PM and AM waveforms versus modulation depth, where the modulation frequency is set to $f_{\rm mod} = 100$mHz for both cases. For the PM case, the waveform is described as

$$h = A\ \sin\left(2\pi\theta(t)t + \phi\right) \tag{5}$$

where A is the waveform amplitude, ϕ is an arbitrary phase and $\theta(t)$ is the instantaneous frequency

$$\theta(t) = f_0 + \Delta f \cos\left(2\pi f_{\rm mod} t\right) \tag{6}$$

where f_0 and Δf are the carrier frequency and modulation depth. From fig.(4) the PM sensitivity is essentially constant within modulation depths in the range $\Delta f \in [1:5]$Hz.

The AM injection is parameterized as

$$h(t) = A(t)\cos\left(2\pi f_0 t\right) \tag{7}$$

where

$$\begin{aligned} A(t) &= \mathrm{A}_0\ \frac{x(t) - k_{\rm mod}}{1 + k_{\rm mod}} \\ x(t) &= \sin\left(2\pi f_{\rm mod} t\right) \end{aligned} \tag{8}$$

where A_0 is the waveform amplitude, $k_{\rm mod}$ is the modulation depth, $f_{\rm mod}$ is the modulation frequency and f_0 is the carrier frequency. From fig.(4) the AM sensitivity is essentially constant within modulation depths in the range $k_{\rm mod} \in [0:1]$. The average response to SG, as shown in fig.(3), is also shown in fig.(4) for comparison.

VI. RESULTS

In this section we present the results of the analysis in terms of upper bounds on GW signals based on the loudest event. These limits are reported in terms of event amplitudes and provide a means to constrain astrophysical populations.

Our initial approach to the problem consisted in measuring the excess power $\Delta\mathcal{P}$ both for the on and off-source segments, and similarly to the search sensitivity, applying software injections to determine an upper bound. For instance, the 90% upper bound on the waveform strength associated to a particular QPO transient would correspond to the injected $h_{\rm rss}$ such that the resulting signal is 90% of the time greater than the on-source signal. This approach, however, can lead to a null or non-physical result: there are cases for which the background is already greater than or equal to 90% of the on-source segment.

To address this problem we used the unified approach of Feldman-Cousins[25], which provides upper confidence limits for null results, two-sided confidence intervals for non-null results and treats confidence limits with restraints on a physical region. In view of the fact that at the time of the hyperflare event only one of the three LIGO detectors was collecting data and that the full detector diagnostic capability was not fully exploited, the lower bounds on the confidence intervals was set to zero.

Table X of ref.[25] was used to place the upper limits of this search. The excess power distribution for the background of each QPO transient was parameterized with a Gaussian PDF, and the Maximum-Likelihood-Estimation (MLE) method was used to estimate the mean μ and standard deviation σ with their relative errors. The on-source excess power segment measure and the lookup table were then used to set 90% confidence intervals.

Tab.(II) presents the results of this search in terms of 90% upper bounds on the GW waveform strength $\mathrm{h}_{\rm rss}^{90\%}$ measured at the time of the observation. The first column of the table indicates the observation we address, with reference to the original measurements shown in tab.(I). The second, third and fourth columns indicate the center frequency, period and duration used in the search. The data quality cut, indicating the threshold cut on power measured in a given tile duration, is shown in the fifth column.

The last three columns, labeled $\mathrm{h}_{\rm rss}$, $\delta\mathrm{h}_{\rm rss}^{\rm syst}$ and $\mathrm{h}_{\rm rss}^{90\%}$, present the results. The first of these, column $\mathrm{h}_{\rm rss}$, places the 90% upper bound and shows the statistical uncertainties in the background estimation (separately). These uncertainties are generated using a Monte-Carlo simulation: a set of means $\hat{\mu}$ and standard deviations $\hat{\sigma}$ are extracted from Gaussian distributed populations of standard deviation $\sigma_{\hat{\mu}}$ and $\sigma_{\hat{\sigma}}$ corresponding to the fit parameter uncertainties. For each $(\hat{\mu}, \hat{\sigma})$ combination and the same on-source excess power measure we used the lookup table in ref.[25] to generate 90% confidence intervals for the quoted upper limit.

The occasional presence of tails, consisting of a couple of events for a total number of events of $<\sim 100$, in the off-source segments introduces a bias in the upper bounds which is presented in the $\delta\mathrm{h}_{\rm rss}^{\rm syst}$ column. This bias is quantified by including and excluding $\pm 3\sigma$ outliers from the fitting procedure and the difference in the upper bounds is shown in the column in question.

Finally the last column represents our 90% upper bound on the waveform strength taken as the amplitude sum of the $\mathrm{h}_{\rm rss}$ value with the upper bound of the statistical uncertainty and the systematic uncertainty $\delta\mathrm{h}_{\rm rss}^{\rm syst}$.

A second source of systematic errors arises from the detector response to GW radiation via the calibration procedure. Taking into consideration the fact that the detector was in commissioning mode, we placed a conservative systematic uncertainty of 25% and all bounds listed in tab.(II) have been increased by this amount.

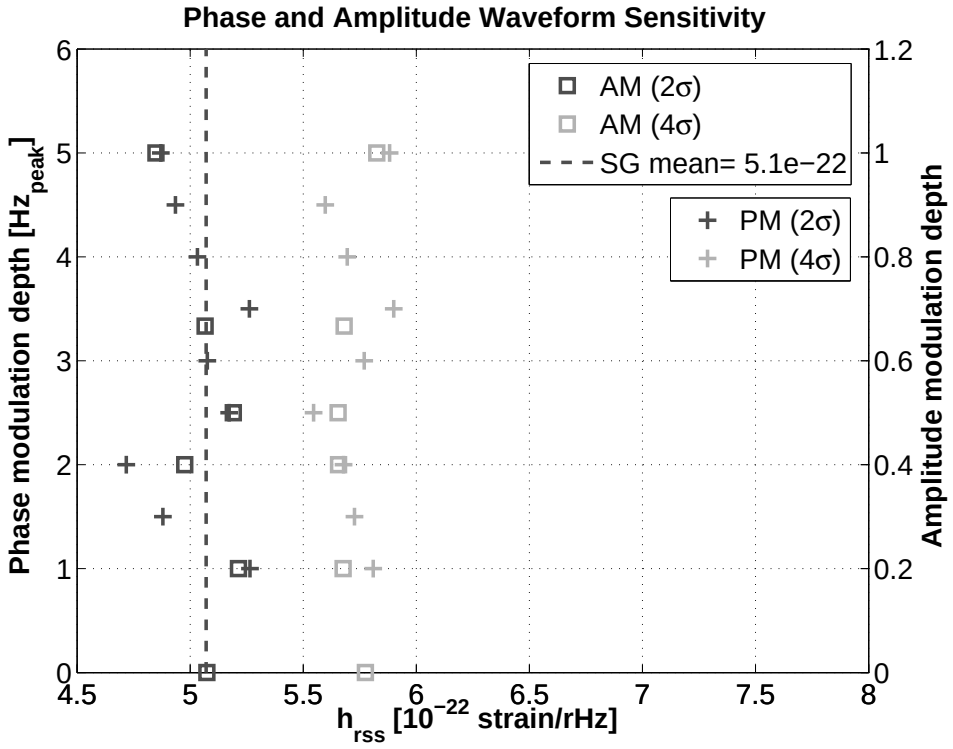

FIG. 4: Search sensitivity to PM (crosses) and AM (squares) waveforms as a function of modulation depth, where for both cases the modulation frequency is set to 100mHz. The sensitivity of the search is essentially constant for the parameter space shown in the figure.

VII. ASTROPHYSICAL INTERPRETATION

In this section we provide a representative GW energy $\mathcal{E}_{\rm gw}^{\rm iso}$ associated to the measured upper bounds $h_{\rm rss}^{90\%}$, shown in tab.(II), cast in terms of a simple source model. In this model we assume that the emission is isotropic with an equal amount of power in both polarization states (circular polarization).

In terms of Sine-Gaussian waveforms with quality factor $Q \gg 1$, the interferometer response to GW radiation can be approximated as

$$\begin{aligned}\left(h_{\rm rss}^{90\%}\right)^2 &= F_+(\theta,\phi,\psi)^2\ h_{+\rm rss}^2 + F_\times(\theta,\phi,\psi)^2\ h_{\times\rm rss}^2 \quad (9)\\ &= h_{+\rm rss}^2\ \Big[\ F_+(\theta,\phi,\psi)^2\ + F_\times(\theta,\phi,\psi)^2\ \Big]\end{aligned}$$

with

$$h_{+\rm rss}^2 = h_{\times\rm rss}^2 \quad (10)$$

where $F_+(\theta,\phi,\psi)$ and $F_\times(\theta,\phi,\psi)$ are the antenna response functions (θ and ϕ are specified by the Right Ascension (RA), Declination (DEC), time and location of the detector and ψ is the polarization angle) and $h_{+\rm rss}^2$ and $h_{\times\rm rss}^2$ represent the waveform energy in the + and × polarization states.

The antenna functions are separable functions in the polarization angle

$$\begin{aligned}F_+(\theta,\phi,\psi) &= P(\theta,\phi)\ \cos 2\psi\ +\ Q(\theta,\phi)\ \sin 2\psi \quad (11)\\ F_\times(\theta,\phi,\psi) &= -Q(\theta,\phi)\ \cos 2\psi\ +\ P(\theta,\phi)\ \sin 2\psi\end{aligned}$$

and eq.(9) simplifies to

$$\left(h_{\rm rss}^{90\%}\right)^2 = h_{+\rm rss}^2\ \Big[\ P(\theta,\phi)^2\ + Q(\theta,\phi)^2\ \Big] \quad (12)$$

In the limit $Q \gg 1$, the wave energy passing through a sphere of radius r centered upon the source can be approximated as

$$\mathcal{E}_{\rm gw}^{\rm iso} = 2\ \frac{\pi^2\ r^2\ c^3\ f_0^2}{G}\ h_{+\rm rss}^2 \quad (13)$$

At the time of the event, the antenna functions are

$$\begin{aligned}Q(\theta,\phi)^2 &= 1.65\times 10^{-1} \quad (14)\\ P(\theta,\phi)^2 &= 8.54\times 10^{-3}\end{aligned}$$

and eq.(13) can be rewritten in terms of solar mass units

$$\begin{aligned}\mathcal{E}_{\rm gw}^{\rm iso} &= 6.63\times 10^{-8} M_{\rm sun} c^2\ \times \quad (15)\\ &\left(\frac{r}{10{\rm kpc}}\right)^2\left(\frac{f_0}{92.5{\rm Hz}}\right)^2\left(\frac{h_{\rm rss}}{5.63\times 10^{-22}/\sqrt{\rm Hz}}\right)^2\end{aligned}$$

Tab.(II) lists the bounds in energy $\mathcal{E}_{\rm gw}^{\rm iso}$ associated to the observed QPOs. It is worth noting that the best energy upper bound is a factor of a few away from the energy emitted in the electromagnetic spectrum (see for example ref.[4]).

Observation	Frequency [Hz]	Period [s]	Bandwidth [Hz]	Duration [s]	Data Quality	h_{rss}	δh_{rss}^{syst} [10^{-22}strain/$\sqrt{\text{Hz}}$]	$h_{rss}^{90\%}$
e,f	92.5	150-260	10	110	125ms, 2σ	$3.43^{+1.23}_{-1.27}$	+0.96	5.63
g		190-260		70		$3.62^{+1.08}_{-0.97}$	+0.93	5.63
d		170-220		50		$6.44^{+0.84}_{-0.96}$	+0.46	7.74
		0-260		260		$6.33^{+3.44}_{-3.34}$	+2.76	12.5
e,f	185.0	150-260	8	110	125ms, 2σ	$11.9^{+1.23}_{-1.38}$	+0.34	13.4
g		190-260		70		$10.2^{+0.98}_{-1.09}$	+0.21	11.4
d		170-220		50		$10.0^{+0.73}_{-0.79}$	+0.30	11.1
		0-260		260		$14.2^{+2.58}_{-3.16}$	-	16.8
h	150.3	0-350	17	350	-	$15.4^{+4.32}_{-5.92}$	-	19.8
h	300.6	0-350	30	350	-	$33.0^{+10.7}_{-15.0}$	-	43.6
i	625.5	50-200	10	150	-	$32.0^{+4.26}_{-4.87}$	-	36.3
l		190-260		70	-	$24.3^{+2.95}_{-3.41}$	-	27.2
		0-260		260	-	$35.2^{+6.57}_{-8.00}$	-	41.8
i	1253.0	50-200	10	150	-	$61.7^{+9.88}_{-11.8}$	-	71.6
l		190-260		70	-	$38.3^{+6.40}_{-7.36}$	-	44.7
		0-260		260	-	$66.9^{+11.0}_{-13.3}$	-	77.9
m	1837.0	230-245	10	15	-	$43.3^{+3.07}_{-3.29}$	-	46.4
		0-245		245	-	$68.6^{+28.1}_{-33.9}$	-	96.7

TABLE II: List of frequencies and observation times used in this analysis with the corresponding results. The first, second and third columns represent the frequency, bandwidth and observation period used in the search. The last two columns list the 90% upper bound results expressed in terms of $h_{\rm rss}$ and GW energy equivalent (see sec.(VII)).

VIII. CONCLUSION

Quasi-Periodic Oscillations have been observed in the pulsating tail of the SGR 1806-20 hyperflare of December 27 2004. The present consensus interprets the event as a dramatic re-configuration of the star's crust and/or magnetic field. In turn, this *starquake* could plausibly excite the star's global seismic modes and the observed QPOs could potentially be driven by the seismic modes. The energetics of the event, the close proximity of the source, and the precise QPO frequencies and bandwidths provided a unique opportunity to measure GWs associated to this phenomena.

At the time of the event only one of the three LIGO detectors was in operation under the *Astrowatch* program. Under this program, data is collected at times of commissioning when the interferometers are in well-established states. Only $\sim$ 2h of data was available for this analysis.

An algorithm was designed to measure the *excess power* deposited in the machine at the time of the event. This algorithm exploits power measures in multiple bands to reject common mode noise sources, such as broadband noise. Power measures in times scales less than 1s are also monitored to reject *fast* signatures inconsistent to the scope of this analysis.

The analysis pipeline was designed and built under the Matlab environment to make this measurement possible. The design was driven by the desire to repeat this measurement for future flares with the ability to use multiple data streams from multiple detectors, focusing on modularity, flexibility, and above all simplicity.

Signals were software injected in the raw data stream to study the analysis sensitivity to different waveform families and parameters. A parameter space was explored under which the search sensitivity is essentially constant. A provision to replace the detector data with white gaussian and stationary noise was included to test the full pipeline and simulate the analysis. The results of the Monte Carlo studies were matched to analytical estimates.

At the time of the event, the strain-equivalent amplitude spectral density of the detector output was a fac-

tor of a few away from the one corresponding to the fourth science run. Under this condition the best upper limit that we place corresponds to the 92.5Hz QPO observed 150s to 260s seconds after the flare. In terms of waveform strength, we place a 90% upper bound of $h_{rss}^{90\%} = 5.63 \times 10^{-22}\mathrm{strain}/\sqrt{\mathrm{Hz}}$, which, in terms of a simple source model, provides a characteristic energy $\mathcal{E}_{gw}^{iso} = 6.63 \times 10^{-8}\mathrm{M_{sun}c^2}$. This is the best upper limit published to our knowledge and represents the first multiple-frequency astero-seismology measurement using a GW detector.

The limits presented here represent GW measures from the state-of-the-art LIGO detectors. At the time of this writing, LIGO is undergoing a data-taking period, referred to as the fifth science run S5[REF], where all three interferometers have reached designed sensitivity. This improvement corresponds to a decrease of ~ 5 in strain-equivalent noise and ~ 25 in terms of GW energetics if such an event would repeat. This estimate excludes the power of cross-correlating data streams from the multiple LIGO detectors.

At the end of the year-long S5 data-taking period, the initial LIGO detectors will be upgraded to an enhanced state[26] which we refer to as Enhanced LIGO. The foreseen improvement will be a factor ~ 2 in strain-equivalent noise. Advanced LIGO would open up the low frequency sensitivity so that low frequency QPOs would be explored and the noise floor would decrease to a factor ~ 10 with respect to initial LIGO. If a second hyper-flare event would occur at the time, the GW energtics at 100Hz would be in the $10^{-10}\mathrm{M_{sun}c^2}$ regime.

[1] P. M. Woods and C. Thompson, ArXiv Astrophysics e-prints (2004), astro-ph/0406133.
[2] E. P. Mazets, S. V. Golentskii, V. N. Ilinskii, R. L. Aptekar, and I. A. Guryan, Nature (London) **282**, 587 (1979).
[3] K. Hurley, T. Cline, E. Mazets, S. Barthelmy, P. Butterworth, F. Marshall, D. Palmer, R. Aptekar, S. Golenetskii, V. Il'Inskii, et al., Nature (London) **397**, 41 (1999), astro-ph/9811443.
[4] K. Hurley, S. E. Boggs, D. M. Smith, R. C. Duncan, R. Lin, A. Zoglauer, S. Krucker, G. Hurford, H. Hudson, C. Wigger, et al., Nature (London) **434**, 1098 (2005), astro-ph/0502329.
[5] P. M. Woods, C. Kouveliotou, M. H. Finger, E. Gogus, C. A. Wilson, S. K. Patel, K. Hurley, and J. H. Swank, ArXiv Astrophysics e-prints (2006), astro-ph/0602402.
[6] A. L. Watts and T. E. Strohmayer, **637**, L117 (2006), astro-ph/0512630.
[7] T. E. Strohmayer and A. L. Watts, ArXiv Astrophysics e-prints (2006), astro-ph/0608463.
[8] G. L. Israel, T. Belloni, L. Stella, Y. Rephaeli, D. E. Gruber, P. Casella, S. Dall'Osso, N. Rea, M. Persic, and R. E. Rothschild, **628**, L53 (2005), astro-ph/0505255.
[9] R. C. Duncan and C. Thompson, **392**, L9 (1992).
[10] R. C. Duncan, **498**, L45+ (1998), astro-ph/9803060.
[11] T. E. Strohmayer and A. L. Watts, ArXiv Astrophysics e-prints (2006), astro-ph/0608463.
[12] P. N. McDermott, H. M. van Horn, and C. J. Hansen, Astrophys. J. **325**, 725 (1988).
[13] A. L. Piro, **634**, L153 (2005), astro-ph/0510578.
[14] B. L. Schumaker and K. S. Thorne, **203**, 457 (1983).
[15] K. Glampedakis and N. Andersson, Phys. Rev. D **74**, 044040 (2006), astro-ph/0411750.
[16] K. Glampedakis, L. Samuelsson, and N. Andersson, **371**, L74 (2006), astro-ph/0605461.
[17] D. M. Palmer, S. Barthelmy, N. Gehrels, R. M. Kippen, T. Cayton, C. Kouveliotou, D. Eichler, R. A. M. J. Wijers, P. M. Woods, J. Granot, et al., Nature (London) **434**, 1107 (2005), astro-ph/0503030.
[18] P. B. Cameron, P. Chandra, A. Ray, S. R. Kulkarni, D. A. Frail, M. H. Wieringa, E. Nakar, E. S. Phinney, A. Miyazaki, M. Tsuboi, et al., Nature (London) **434**, 1112 (2005), astro-ph/0502428.
[19] S. Corbel and S. S. Eikenberry, **419**, 191 (2004), astro-ph/0311313.
[20] N. M. McClure-Griffiths and B. M. Gaensler, **630**, L161 (2005), astro-ph/0503171.
[21] É. É. Flanagan and S. A. Hughes, Phys. Rev. D **57**, 4535 (1998), gr-qc/9701039.
[22] É. É. Flanagan and S. A. Hughes, Phys. Rev. D **57**, 4566 (1998), gr-qc/9710129.
[23] W. G. Anderson, P. R. Brady, J. D. E. Creighton, and E. E. Flanagan, Phys. Rev. D **63**, 042003 (2001).
[24] S. J. Schwartz, S. Zane, R. J. Wilson, F. P. Pijpers, D. R. Moore, D. O. Kataria, T. S. Horbury, A. N. Fazakerley, and P. J. Cargill, **627**, L129 (2005), astro-ph/0504056.
[25] G. J. Feldman and R. D. Cousins, Phys. Rev. D **57**, 3873 (1998), physics/9711021.
[26] P. Fritschel, R. Adhikari, and R. Weiss, LIGO Technical Note (2005), www.ligo.caltech.edu/docs/T/T050252-00.pdf.
[27] http://gcn.gsfc.nasa.gov/gcn3/2920.gcn3
[28] http://gcn.gsfc.nasa.gov/gcn3/2936.gcn3